ISSN: 2579-5821 (Print)
ISSN: 2579-5546 (Online)
URL address: http://journal.unhas.ac.id/index.php/geocelebes
DOI: 10.20956/geocelebes.v8i1.33969

Jurnal Geocelebes Vol. 8 No. 1, April 2024, 71 – 82

1D Audio Magnetotelluric Modelling for Deep Aquifer Identification in the Lava Fan Area of Haruman Peak, Malabar Mountains

Nabilah Rahmawati[1], Nabila Putri Kusuma[1], Shofie Dzakia Hanifah[1], G.M. Lucki Junursyah[2], Asep Harja[1]*

[1]Department of Geophysics, Padjadjaran University, Jl. Raya Bandung-Sumedang KM. 21, Jatinangor, Sumedang, West Java, 45363
[2]Center for Geological Survey, Geological Agency, Ministry of Energy and Mineral Resources, Bandung, Indonesia

*Corresponding author. Email: asep.harja@geophys.unpad.ac.id

Manuscript received: 14 March 2024; Received in revised form: 20 April 2024; Accepted: 28 April 2024

Abstract

The Malabar Mountains area acts as a catchment and infiltration zone for rainwater. Haruman Peak is the location of one of these areas. Information on the well-preserved depth of the shallow aquifer at 40 meters reinforces this. This research reviews the results of subsurface 1D resistivity structures from AMT data to obtain information on the depth of deep aquifers on the western slope of the Haruman Peak Lava Fan, Haruman Mountains. 1D modelling shows an aquifer at depth of 140.56-2080.07 meters with resistivity ranging from 5.25-68.08 Ωm. At depths of 453.32 m (HR02), 530.8 m (HR03), 1464.97 m (HR01), and 2080.07 m (HR02), interbedded tuff-andesite with minor pumice identifies the deep aquifer. In addition, a depth of 140.56 m (HR02) with a resistivity value of 68.08 Ωm indicates a shallow aquifer. Looking at the elevation of the Bandung Basin, water from aquifers located at elevations > 700 meters above sea level will flow into the Bandung Basin.

Keywords: 1D; audio magnetotelluric; deep aquifer; Haruman peak; subsurface resistivity structure.

Citation: Rahmawati, N., Kusuma, N. P., Hanifah, S. D., Junursyah, G. M. L., & Harja, A. (2024). 1D Audio Magnetotelluric Modelling for Deep Aquifer Identification in the Lava Fan Area of Haruman Peak, Malabar Mountains. *Jurnal Geocelebes*, 8(1): 71–82, doi: 10.20956/geocelebes.v8i1.33969

Introduction

Mount Malabar is a type B volcano located south of Bandung and forms the boundary between the Bandung plateau (700 m) to the north and the Pangalengan plateau (1400 m) to the south. The Malabar Mountain complex is a crucial catchment and rainwater infiltration zone. Haruman Peak is one of the main infiltration zones of the Bandung–Soreang Groundwater Basin located on the western side of the Malabar Mountain range (Harja et al., 2021). The mountain slopes that lead into the Bandung Basin support this claim, as stated by Suhari and Siebenhüner (1993). Furthermore, recent studies by Harja et al. (2021, 2023) have provided clear and precise information on the depth of shallow aquifers at 40 meters, which are still well-preserved.

Information on the existence of deeper aquifers is not yet clearly known. Therefore, a deep investigation of geophysical measurement is needed, one of which uses the Audio Magnetotelluric (AMT) method that can detect resistivity variations from tens of meters to tens of kilometers (Gomo, 2023). This method utilizes lightning activity in the ionosphere as its source with a frequency range from 0.1 Hz–10 kHz (Constable, 2016), which is both environmentally friendly and easy to use. The AMT method is used in hydrology to determine aquifer thickness and depth, to define the deepest geological strata, and to characterize groundwater migration (Li et

al, 2021; Montahaei, 2022; Tripathi et al., 2019; Xu et al., 2020; 2023; Zaher et al., 2021). The expected result of using AMT method in this research is to determine the presence of deeper aquifers based on the contrast of rock resistivity values modelled in 1D.

Geology of the research area

The research was focused on the western slope of Haruman Peak, Malabar Mountains, West Java, with three points including HR01 (7°8'20.10"S and 107°34'48.36"E), HR02 (7°8'24.78"S and 107°34'51.48"E), and HR03 (7°8'28.98"S and 107°34'50.14"E) (Figure 1). The description of stratigraphy and lithology in the research area is based on the Geological Map of Garut and Pameungpeuk Quadrangle, Java (Alzwar et al., 1992). The geology of the measuring region is separated into volcanic rock units and surface sediment units, with Tertiary volcanic rocks overlain by Quaternary volcanic rocks that deposit surface sediment units. The rock units exposed around the AMT research area are Miocene to Holocene age rocks, including the Beser Formation (Tmb), with a thickness of about 500–1000 m consisting of tuffaceous breccia and lavas of andesitic to basaltic composition and containing pumice fragments; and the Waringin-Bedil Andesite, Old Malabar (Qwb), with a thickness of about 600 m consisting alternation of lavas, breccia, and tuffs.

The Beser Formation (Tmb) is a Late Miocene rock unit spread northwest of the Garut and Pameungpeuk Quadrangle. It is overlapped unconformity by the Pliocene Tufaan Breksi Formation (Tpv), consisting of breccia, tuff, and sandstone, and has a thickness of about 600–700 m. Furthermore, there is the Old Undecomposed Volcanic Rock Formation (Qtv) with a thickness of 500–800 m, Plio-Pleistocene age, which overlaps the Tufaan Breccia Formation (Tpv) and overlaps incongruously with Old Quaternary Volcanic Rocks. The Qtv Formation products are assumed to be the product of eruptions with undecomposable sources, including fine to coarse tuff, pumice tuff breccia, and andesite lava.

Above the Qtv formation settled the Pleistocene-aged Waringin Bedil Andesite unit, Old Malabar (Qwb). Then, the rock unit is overlain by the Undifferentiated Efflata Deposits of Old Volcanics (Qopu), with a thickness of about 400 m consisting of fine to coarse tuff, tuffaceous breccia, and old laharic deposits, and formed in the Pleistocene era. The products of the formation filled the valley of the Old Malabar volcanic depression and formed the Pangalengan plateau. After that, there was a deposition of Pleistocene rocks with a thickness of 1400 m above it, which is the Malabar-Tilu Volcano Rock Unit (Qmt) consisting of tuff, laharic breccia containing minor of pumice, and lavas. The unit is overlapped by the Tilu Lava Formation (Qtl) and its constituent rocks come from G. Malabar I/Ipis, G. Malabar II/Puncakbesar, and G. Tilu. Lastly, the Tilu Lava Formation (Qtl) that appears to the southwest of the Old Malabar volcanic depression is composed by andesitic lava and basaltic andesite formed in the Pleistocene epoch.

Based on Garut and Pameungpeuk Quadrangle, the research area located south of a northwest-southeast trending fault. Faults can be an outlet or entry of surface water into the aquifer layer below the surface and can withstand the direction of water flow that should be (Keegan-Treloar et al., 2022; Kurniawan et al., 2022).

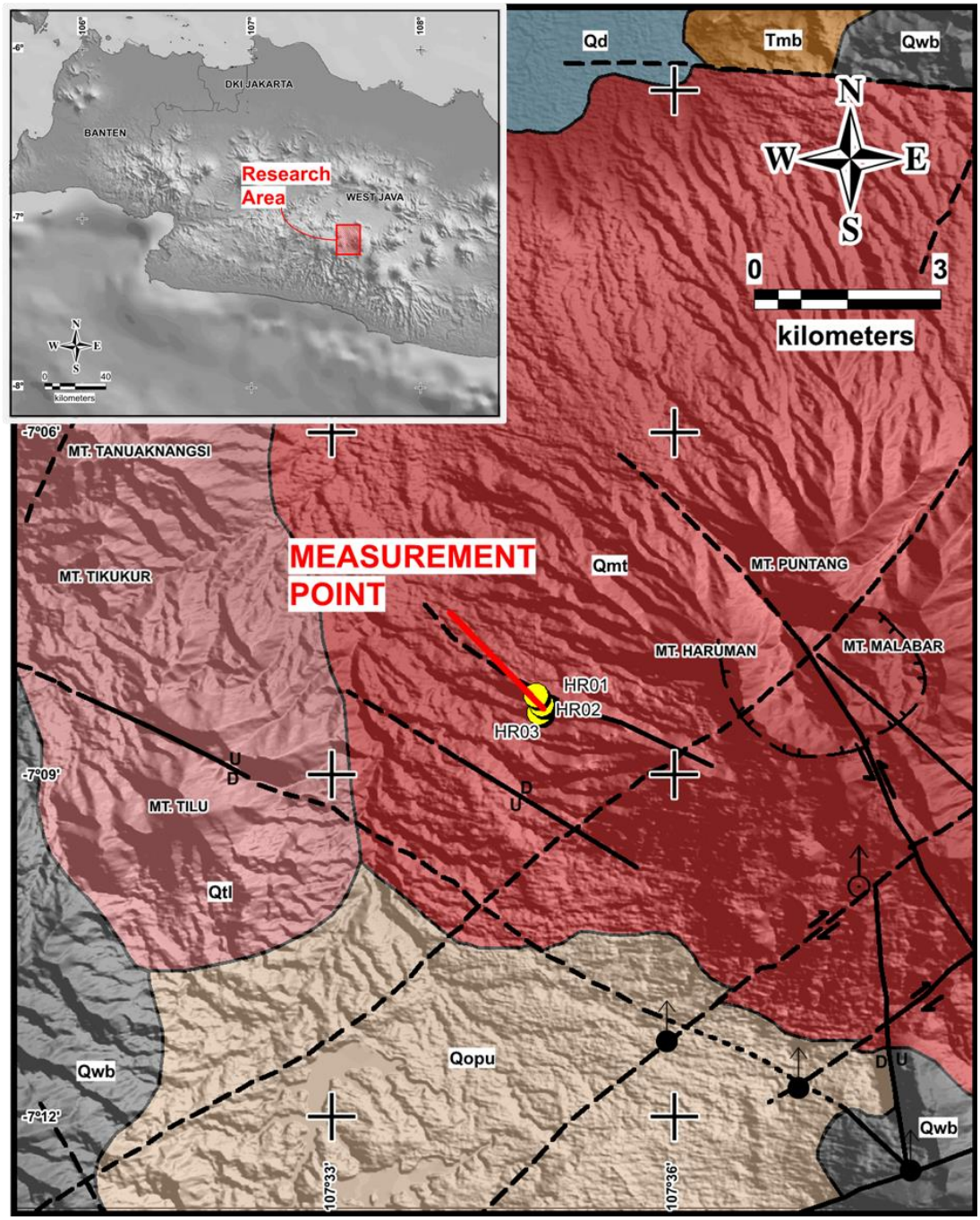

Figure 1. Geologic Map of Research Area (modification of Garut and Pameungpeuk Map, Java by Alzwar et al., 1992).

Research Methods

AMT method measurements with the recorder main unit MTU-5A were carried out at three points on the western slope of the Malabar Mountains, precisely in Warjabakti Village, Cimaung District, Bandung Regency, West Java. The distance between HR01 and HR02 is about 175 meters, while the distance between HR02 and HR03 is about 135 meters. The data generated from the AMT acquisition is in the form of magnetic and electric field intensity variation data in the time domain (Hidayat et al., 2021). Each point is measured using vector measurement mode for 30 minutes. The length of the AMT measurement makes the data obtained in the frequency range of 0.35 Hz to 10400 Hz (Wu et al., 2023). The data is then processed to obtain an apparent resistivity curve, which is calculated based on the ratio

of the size of the electric field (E) and the magnetic field (H) (Figure 2). The comparison is called the Cagniard equation (Equation 1) (Cagniard, 1953).

$$\rho_a = \frac{1}{5f}\left|\frac{E_x}{H_y}\right|^2 \quad (1)$$

The steps of the procedure are Fast Fourier Transform, Robust Processing, and cross-power selection (XPR) (Kurniawan et al., 2019). Fast Fourier Transform is a method used to transform data from the time domain to the frequency domain. The next step is robust processing, which tries to detect, eliminate, and decrease outliers. This step performs iterative weighting of residuals to lower the weight of outliers. The robust process considers the coherence of each robust parameter's results. Coherence is a real number with a dimension ranging from 0 to 1, where 1 indicates a perfectly coherent transmission. The robust process has three types of cross-power parameters, such as No Weight—doing the same weighting at each frequency, Rho Variance—doing high weighting on the type resistance that has as many snippets as the desired cross-power value, and Ordinary Coherence—doing high weighting at frequencies with good coherence between the H and E components (Junursyah et al., 2020). The Ordinary Coherence parameter has the highest coherence value among the three cross-power parameters, with coherence greater than 70%. The apparent resistivity and phase curves generated in the robust process usually have random patterns due to noise in the recorded data, therefore XPR is carried out to smoothen the curve. The XPR is carried out by selecting high-weight XPR data and eliminating low-weight XPR data (Figures 2, 3, and 4).

Curve trend analysis is the next step that removes data far from the curve trend (outliers). The deviant curve data is affected by noise in the initial data, robust results, and XPR. The maximum depth is then calculated based on the skin depth using Equation 2.

$$\delta = 503\sqrt{\frac{\rho}{f}} \quad (2)$$

After the curve trend analysis, the data is modeled in 1D with Occam inversion to calculate the maximum depth based on resistivity variation. The Occam inversion serves to minimize the roughness level of the resulting model. The results from the inversion calculation of the model will be smoother, establishing the fitting process of field data (Constable et al., 1987).

Furthermore, the data is analyzed to determine the dimensionality of the subsurface resistivity structure, known as skewness analysis. This analysis to determine if there are deviations or distortions in the impedance tensor in magnetotelluric data (Junursyah, 2022). There are two techniques for skewness analysis: Swift skew and Bahr skew. Swift skew is the ratio between the diagonal components (Z_{xx} and Z_{yy}) and the non-diagonal components (Z_{xy} and Z_{yx}) of the impedance tensor (Equation 3). If the $skew_{Swift}$ value > 0.3 implies 3D or noise. If the $skew_{Swift}$ value < 0.3, it suggests 1D or 2D (Pranata et al., 2017). Swift skew is a one-dimensional data analysis for determining whether the underlying electrical structure is distorted or not. The skewness value will look deviated if the impedance tensor has telluric distortion (Xiao et al., 2011; Tripathi et al., 2019).

$$Skew_{Swift} = \left|\frac{Z_{xx} + Z_{yy}}{Z_{xy} - Z_{yx}}\right| \quad (3)$$

Bahr skew is a calculation developed on the value of phase sensitivity skewness (η) or regional skew by considering telluric distortion in the impedance tensor (Bahr, 1991). The phase sensitivity slope can be determined using Equation (4).

$$\eta = \frac{\sqrt{2\left|ReZ_{xx}\cdot ImZ_{yx} - ReZ_{yy}\cdot ImZ_{xy} + ReZ_{xy}\cdot ImZ_{yy} - ReZ_{yx}\cdot ImZ_{xx}\right|}}{|Z_{xy} - Z_{yx}|} \quad (4)$$

Re represents the real part of a complex number, while Im represents the imaginary

part. If the value of $\eta > 0.3$, it suggests 3D inductive effect, while $\eta = 0$ suggests an ideal values of 1D-2D electrical structure. A value of $\eta < 0.3$ implies the response of 2D structure (Xiao et al., 2011). A value of less than 0.3 indicates a regionally 2D structure, but it is not sufficient (Tripathi et al., 2019). In this research, the technique used in dimensionality analysis is Bahr skew to clarify the subsurface structure. Research flow chart can be seen in Figure 6.

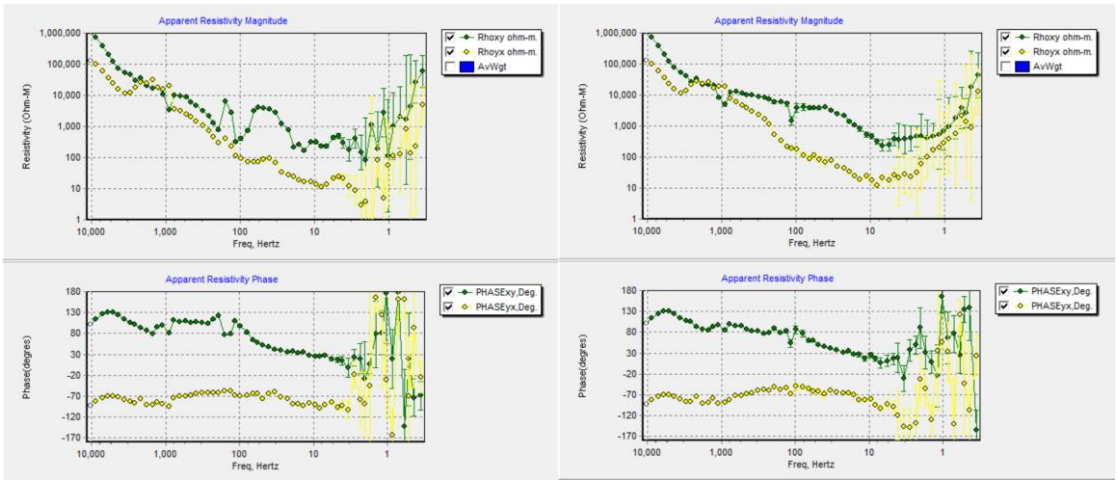

Figure 2. Comparison of the apparent resistivity curve and phase at HR01 before (left) and after XPR (right).

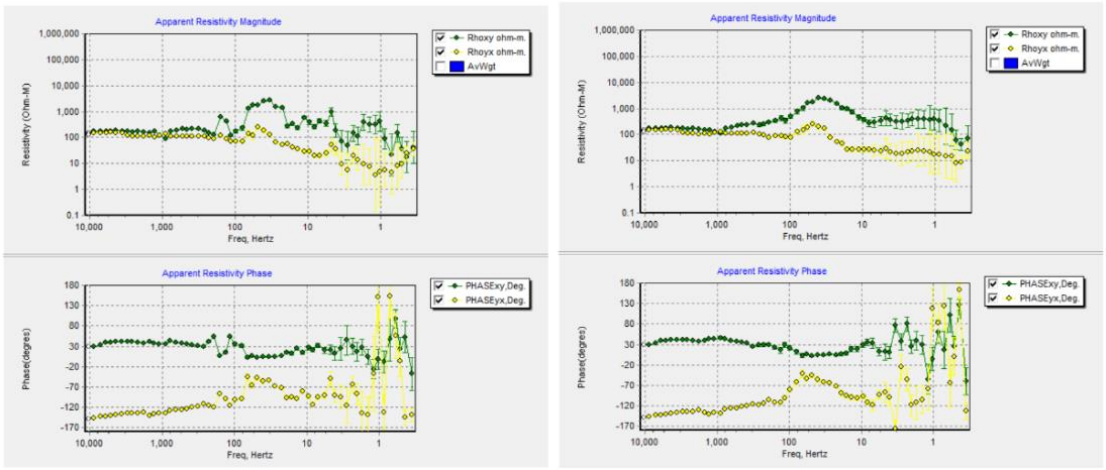

Figure 3. Comparison of the apparent resistivity curve and phase at HR02 before (left) and after XPR (right).

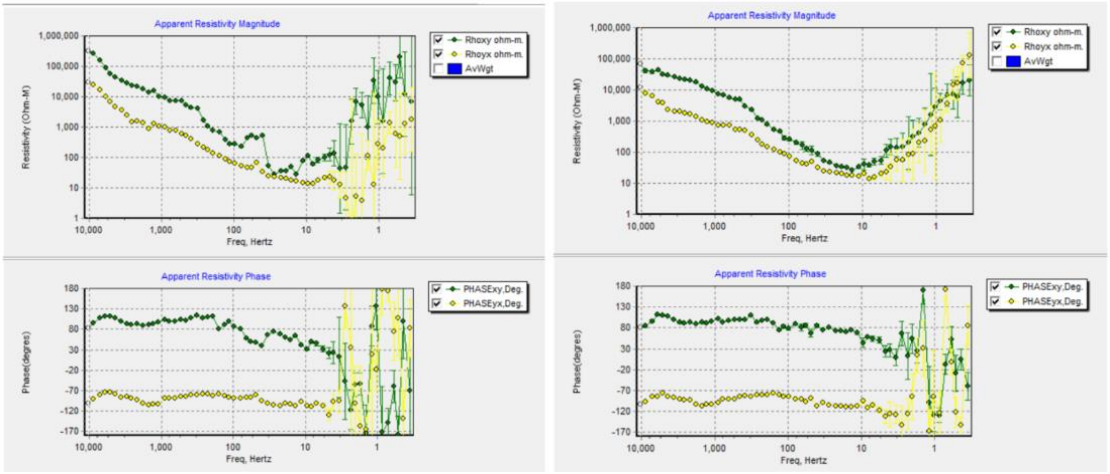

Figure 4. Comparison of the apparent resistivity curve and phase at HR03 before (left) and after XPR (right).

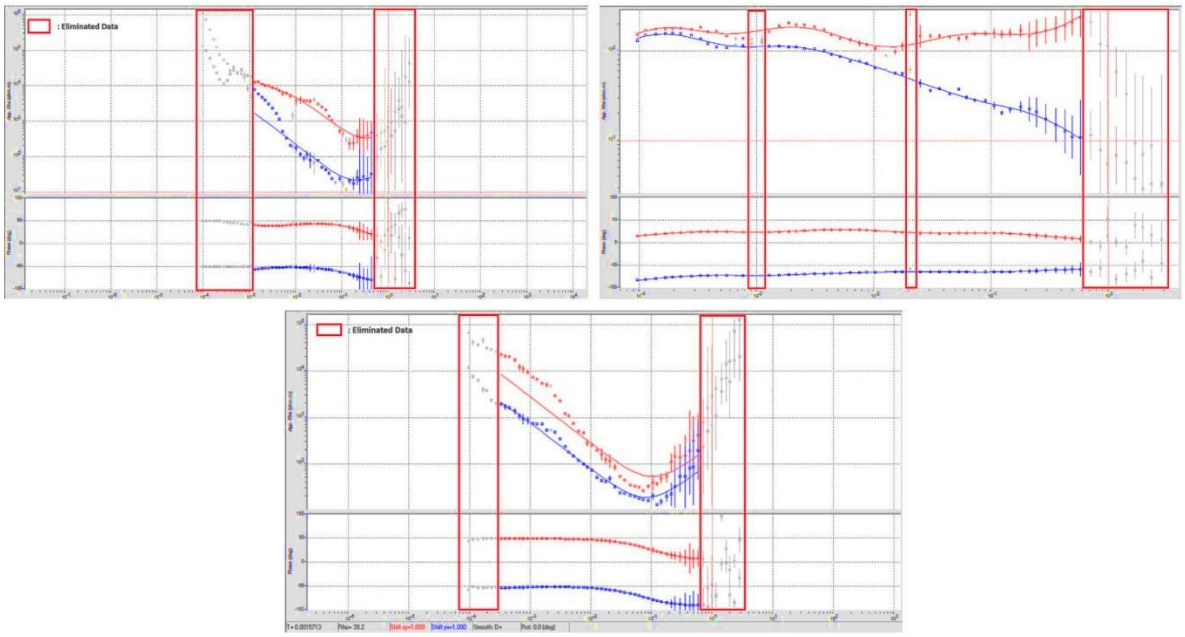

Figure 5. The apparent resistivity and phase curves over period at HR01 (a), HR02 (b) and HR03 (c) showing the elimination of outliers based on curve trend analysis.

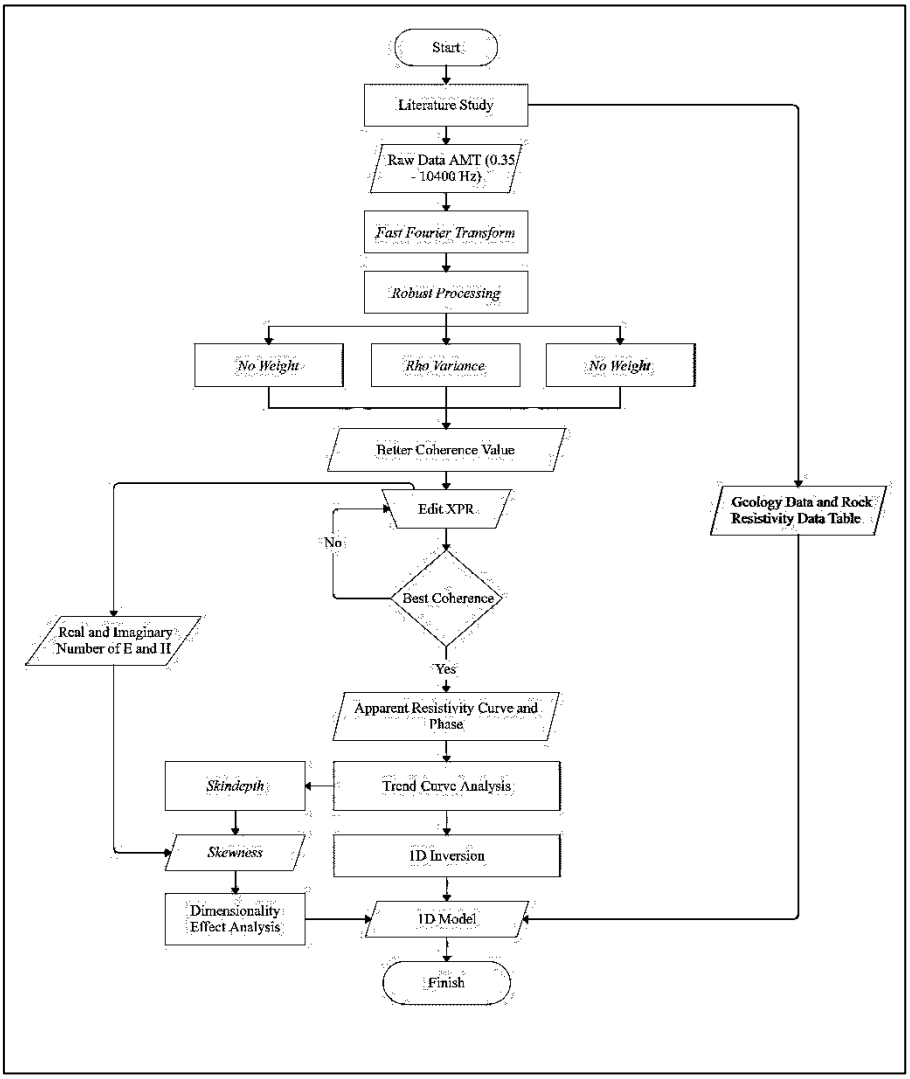

Figure 6. Flow chart from process, data analysis, to 1D modelling (modification from Junursyah et al., 2021; 2023).

Results and Discussion

Data was processed in 1D inversion modelling (Figure 7) using invariant mode (combined mode TE and TM). The analysis and interpretation of 1D modelling results will be correlated with stratigraphic models (Figure 8) regarding the relationship between rock resistivity values in general (Figure 9) and formation unit information on the Geological Map of Garut and Pameungpeuk Quadrangle, Java. According to Figure 8, the increase or decrease in resistivity values as depth increases shows the presence of different lithological formations or arrangements.

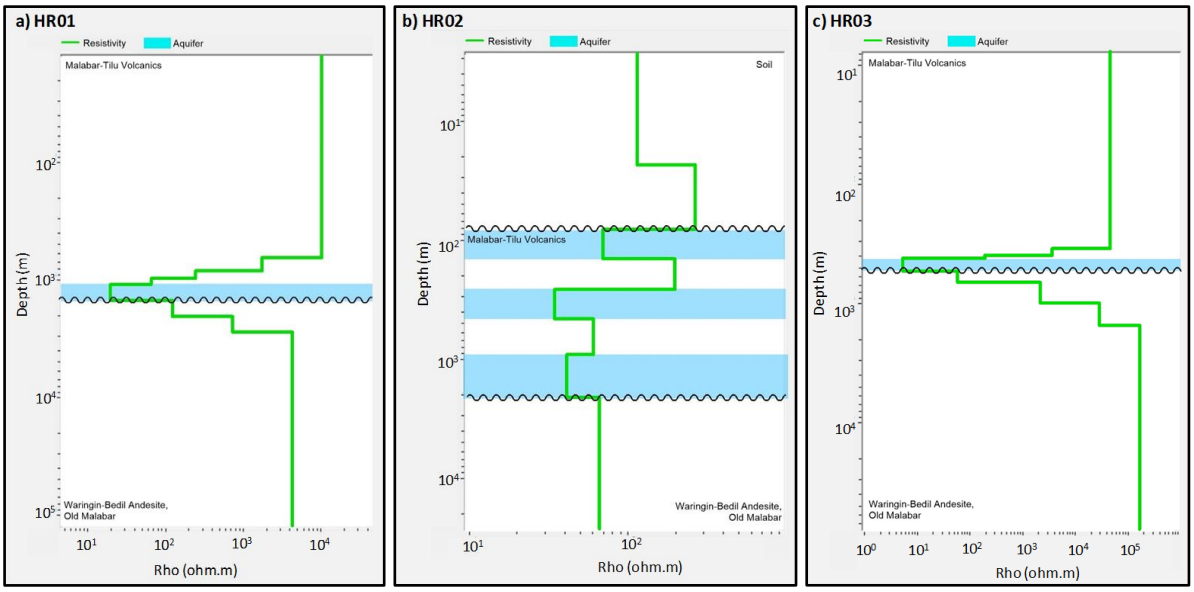

Figure 7. Results of 1D inversion of AMT data at a) HR01, b) HR02, and c) HR03.

DESCRIPTION		AGES	THICK (m)	COMPONENT	RANGE VALUES (Ωm)		AVERAGE (Ωm)	1D MODEL (Ωm)
Qmt	Malabar-Tilu Volcanics	Pleistocene	1400 m	Andesitic lithic tuffs with a minor amount of pumice Laharic breccia with a minor amount of pumice Lavas	709	21500	11,105	
Qopu	Undifferentiated Efflata Deposits of Old Volcanics	Pleistocene	400 m	Fine to coarse dacitic crystalline tuff Tuffaceous breccia Old laharic deposits	1014	7250	4,132	
Qwb	Waringin-Bedil Andesite, Old Malabar	Pleistocene	600 m	Lavas Breccia Tuff	709	21500	11,105	
QTv	Undifferentiated Old Volcanics	Plio-Pleistocene	500 - 800 m	Fine crystalline tuff Tuff breccia Lavas	372	19750	8,579	
Tpv	Tuffaceous Breccia	Pliocene	600 - 700 m	Breccia Fine to coarse tuff Lithic tuff Sandstone	1146	5875	3,511	
Tmb	Beser Formation	Late Miocene	500 - 1000 m	Tuffaceous breccia Lithic tuff Lavas of andesitic to basaltic	405	20583	8,904	

Figure 8. Stratigraphic Model of Haruman Peak, Malabar Mountains Area and Its Surroundings Based on the Range of Rock Resistivity Values in Figure 9 and Formation Information on the Geological Map of Garut and Pameungpeuk Quadrangle, Java.

The results of modelling the 1D resistivity structure shown in Figure 7a., obtained a depth of up to 2704.98 meters with a variation in resistivity values of 19.1 Ωm to 10103.77 Ωm. Layers 1 to 5 decreased resistivity values from 10103.77 Ωm to 19.10 Ωm at a depth of 1464.97 meters. In layers 6-8, the resistivity value reaches 4160.19 Ωm at a depth of >2704.8 meters. When viewed from the change in resistivity value and depth, layers 1 to 5 are predicted as Malabar Tilu Volcanic Rock (Qmt), which overlies the unconformity of Waringin-Bedil Andesite Unit, Old Malabar (Qwb) in layers 6 to 8. Layer 5 has a lower resistivity value and is thought to be

filled with fluid, whereas layers 1-4 and 6-8 have impermeable qualities, as shown by a higher resistivity value than layer 5. The higher the resistivity value, the more massive or dense the rock. Hence, layer 5, at the HR01 has the potential to be an aquifer comprised of tuff-andesite and a minor of pumice. When viewed from the lithological properties and types of water-carrying layers (Kodoatie, 2021), the aquifer at the HR01 is identified as confined aquifer with impermeable upper and lower layers.

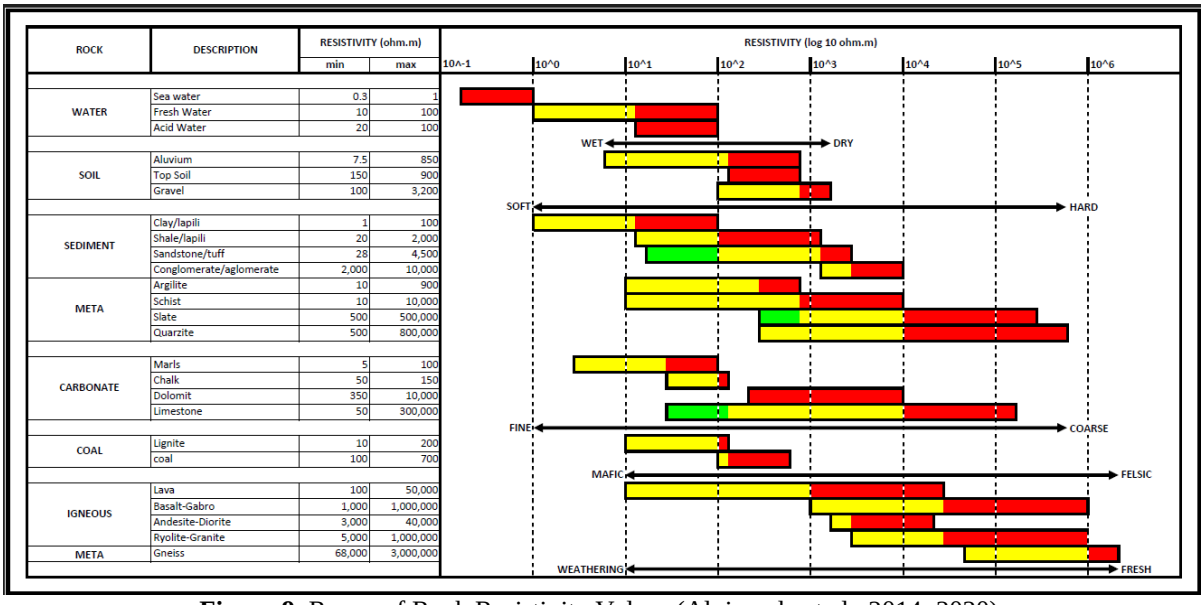

ROCK	DESCRIPTION	RESISTIVITY (ohm.m) min	RESISTIVITY (ohm.m) max
WATER	Sea water	0.3	1
	Fresh Water	10	100
	Acid Water	20	100
SOIL	Aluvium	7.5	850
	Top Soil	150	900
	Gravel	100	3,200
SEDIMENT	Clay/lapili	1	100
	Shale/lapili	20	2,000
	Sandstone/tuff	28	4,500
	Conglomerate/aglomerate	2,000	10,000
META	Argilite	10	900
	Schist	10	10,000
	Slate	500	500,000
	Quarzite	500	800,000
CARBONATE	Marls	5	100
	Chalk	50	150
	Dolomit	350	10,000
	Limestone	50	300,000
COAL	Lignite	10	200
	coal	100	700
IGNEOUS	Lava	100	50,000
	Basalt-Gabro	1,000	1,000,000
	Andesite-Diorite	3,000	40,000
	Ryolite-Granite	5,000	1,000,000
META	Gneiss	68,000	3,000,000

Figure 9. Range of Rock Resistivity Values (Alviyanda et al., 2014; 2020).

Based on Figure 7b., 1D inversion modelling obtained depths of up to 2080.07 meters with variations in resistivity values of 34.2 to 259.31 Ωm. The resistivity value in layers 1 and 2 increased from 114.82 Ωm to 259.31 Ωm at a depth of 80.32 meters. When viewed from the correlation of resistivity values and depth in Figure 8, layers 1 and 2 can be predicted as soil layers formed due to the physical-chemical weathering process of rocks, biological activities of organisms, and a long-term climate (Kalev & Toor, 2018). Different things happen in layers 3 to 8, where resistivity values fluctuate as depth increases. The resistivity value in layer 3 reaches 68.08 Ωm, increases significantly to 195.06 Ωm in layer 4, and decreases sharply to 34.2 Ωm in layer 5. Furthermore, resistivity rises again in layer 6 with a value of 59.94 Ωm but falls back in layer 7 to 40.65 Ωm before finally reaching 65.44 Ωm in layer 8. The resistivity value of rocks that fluctuate with increasing depth illustrates the complexity of the constituent rocks and other contents in each layer. Based on Figure 8, layers 3 to 7 reaching a depth of 2080.07 meters can be predicted as the Malabar-Tilu Volcano Rock Unit (Qmt), which overlies the unconformity Waringin-Bedil Andesite Unit, Old Malabar (Qwb) in layer 8. If there is a drop in resistivity value in layers 3, 5, and 7, this may indicate the possibility of other content, such as fluid, in these layers. Hence, layers 3, 5, and 7 at the HR02 can be said to have the potential to be aquifers composed of tuff-andesite with a minor pumice content. Based on lithological properties and types of water-carrying layers (Kodoatie, 2021), aquifers in layer 3 include *unconfined aquifers*, which have only one watertight boundary layer at the bottom and only groundwater levels at the top (*soil*). The aquifers in layers 5 and 7 are identified as confined aquifers, where the upper and lower layers are impermeable.

The results of modelling the 1D resistivity structure shown in Figure 7c., obtained a depth of up to 1488.83 meters with a variation in resistivity values between 5.25 to 157470 Ωm. Based on the correlation of resistivity and depth values in Figure 8, layers 1–4 are predicted as Malabar Tilu Volcano Rock Unit (Qmt) based on the correlation of resistivity and depth data in Figure 8. These comprised andesitic lithic tuffs with a minor amount of pumice, breccia, and lavas. In addition, layers 5-8 are predicted as Waringin-Bedil Andesite Units, an Old Malabar (Qwb) formation comprised of lavas, breccia, and tuff rocks. Layer 4 has a low resistivity (5.25 Ωm) compared to other layers, indicating it is an aquifer layer comprised of tuff-andesite rock with a minor pumice content. When viewed from the lithological properties and types of water-carrying layers (Kodoatie, 2021), the aquifer at the HR03 is a type of *confined aquifer*.

According to Oktariadi et al. (2021), the Bandung Basin is located between 650 and 700 meters above sea level. Thus, water from aquifers at 140.56 m (HR02), 453.32 m (HR02), and 530.8 m (HR03) are predicted to flow into the Bandung Basin.

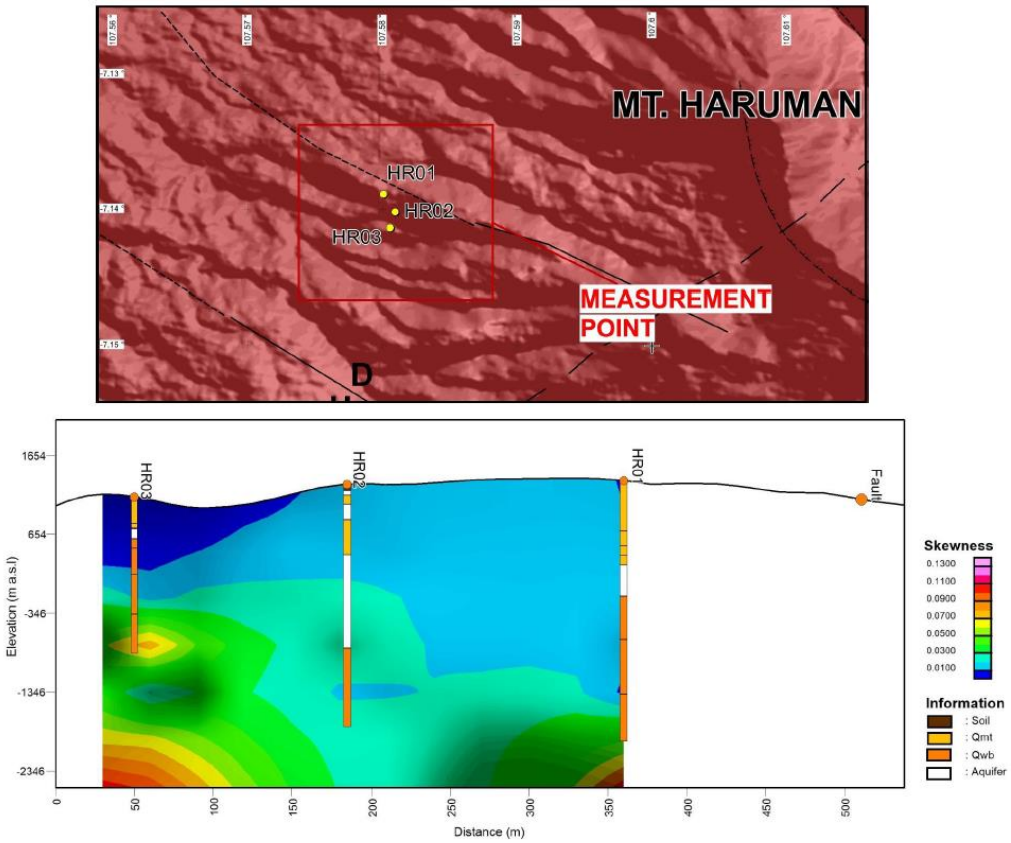

Figure 10. Bahr Skewness Cross-section.

Another step is dimensionality analysis, which aims to clarify the subsurface resistivity structure under research. Based on the results of the dimensionality analysis of AMT data, the Bahr Skew has value variation of 0.01 - 0.13 (Figure 10). The skewness value of the aquifer layer at HR01 ranges from 0.01 - 0.02 (light blue), the aquifer layer at HR02 has two skewness values ranging from 0.01 - 0.02 (light blue) and 0.02 - 0.03 (light green), and the skewness value of the aquifer layer at HR03 ranges from 0 to 0.01 (dark blue). The effect of 3D dimensionality on data is defined by a skewness value (η) > 0.3, while $\eta < 0.3$ implies the 2D dimensionality effect. The ideal condition of 1D-2D *electrical structure* is indicated by $\eta = 0$ (Xiao, 2011). Hence, the aquifer layer in the 1D model interpretation indicates that it is

unaffected by the dimensionality effect. In the skewness cross-section, there is a slight dimensionality effect in the subsurface of measuring points HR01 and HR03. Geological features are thought to be the cause of this; however, it does not affect the surrounding aquifers.

Conclusion

Deep aquifer (confined aquifers) with resistivity values of 5.25 - 40.65 Ωm were identified at depths of 453.32 m (HR02), 530.8 m (HR03), 1464.97 m (HR01), and 2080.07 m (HR02) with lithology in the form of andesite-tuff with minor of pumice. In addition, an unconfined aquifer was also identified at the HR02 point at a depth of 140.56 m with a resistivity value of 68.08 Ωm. Bandung Basin is located between 650 and 700 meters above sea level (m.a.s.l.), and water from aquifers that have an altitude >700 meters above sea level is expected to flow into the Bandung Basin. Water from aquifers located at depths of 140.56 m (HR02), 453.32 m (HR02), and 530.8 m (HR03) has the potential to flow into the Bandung Basin.

Acknowledgements

The author expresses his gratitude to the Geological Survey Center for its role and facilities in the process of acquiring AMT data in Haruman, to M. Riyan Maulana and colleagues for their assistance in completing this research, as well as to the Academic Leadership Grant (ALG) and Unpad Lecturer Competency Research (RKDU) for their support of this research.

Author Contribution

The acquisition process was carried out by all authors with the assistance of the Geological Survey Center and Asep Harja. Data processing was carried out by Nabilah R. and G. M. Lucki Junursyah. All authors discussed, interpreted, and wrote the manuscript.

Conflict of Interest

The authors declare no conflict of interest.

References

Alviyanda, Junursyah, G. M. L, Gumilar, I. S., & Mardiana, U. (2014). Interpretation of Subsurface Structure in Tertiary Sediment Based on Magnetotelluric Data, South Buton area. *Proceedings of the Indonesian Petroleum Association, 38th Annual Convention and Exhibition*, Jakarta.

Alviyanda, Junursyah, G. M. L., & Sumintadireja, P. (2020). Stratigraphic Model of East Biak Based on Magnetotelluric Data. *Journal of Mathematical & Fundamental Sciences*, 52(2), 232–249. https://doi.org/10.5614/j.math.fund.sci.2020.52.2.7

Alzwar, M., Akbar, N., & Bachri, S. (1992). *Peta Geologi Lembar Garut dan Pameungpeuk, Jawa, Skala 1:100.000*. Pusat Penelitian dan Pengembangan Geologi.

Bahr, K. (1991). Geological Noise in Magnetotelluric Data: A Classification of Distortion Types. *Physics of the Earth and Planetary Interiors*, 66(1-2), 24–38. https://doi.org/10.1016/0031-9201(91)90101-M

Cagniard, L. (1953). Basic Theory of the Magneto-Telluric Method of Geophysical Prospecting. *Geophysics*, 18(3), 605–635. https://doi.org/10.1190/1.1437915

Constable, S. C., Parker, R. L., & Constable, C. G. (1987). Occam's Inversion: A Practical Algorithm for Generating Smooth Models from Electromagnetic Sounding Data. *Geophysics*, 52(3), 289–300. https://doi.org/10.1190/1.1442303

Constable, C. (2016). Earth's Electromagnetic Environment. *Surveys in Geophysics*, 37, 27–45.

https://doi.org/10.1007/s10712-015-9351-1

Gomo, M. (2023). Use of Electric Potential Difference in Audio Magnetotelluric (AMT) Geophysics for Groundwater Exploration. *Groundwater for Sustainable Development*, 20, 100864. https://doi.org/10.1016/j.gsd.2022.100864

Harja, A., Ma'arif M., F. R., Nanda, M. D., Duvanovsky, D. A., Tangke, R., Shafa, Z. I., Fillsani, S., Gunawan, I., & Susanto, K. (2021). Studi Hidrogeofisika Gunung Malabar Sebagai Gunung Tertinggi pada Sistem Hidrologi Cekungan Bandung. *Jurnal Geologi dan Sumberdaya Mineral*, 22(4), 223–230. https://doi.org/10.33332/jgsm.geologi.v22i4.654

Harja, A., Aprilia, B. A., Susanto, K., & Fitriani, D. (2023). Identifikasi Zona Akuifer Menggunakan Metode Resistivitas-DC di Daerah Kipas Lava Pegunungan Malabar Kabupaten Bandung Jawa-Barat. *JIIF (Jurnal Ilmu dan Inovasi Fisika)*, 7(1), 49–57. https://doi.org/10.24198/jiif.v7i1.43216

Hidayat, H. Setiawan, J. J., Ibrahim, A., Marjiyono, M., & Junursyah, G. M. L. (2021). Studi Magnetotelurik (MT) Untuk Mendelineasi Potensi Regional Gas Serpih bawah Permukaan Berdasarkan properti Tahanan Jenis di Cekungan Kutai, Kalimantan Timur. *Jurnal Geologi Dan Sumberdaya Mineral*, 22(2), 107–114. https://doi.org/10.33332/jgsm.geologi.v22i2.571

Junursyah, G. M. L., Prabowo, A., & Hidayat, W. (2020). Analisis Kualitas Data Magnetotelurik Berdasarkan Parameter Koherensi Studi Kasus: Data Magnetotelurik Di Daerah Bandung, Jawa Barat. *Jurnal Mineral Energi dan Lingkungan*, 4(2). 78–83. https://doi.org/10.31315/jmel.v4i2.3679

Junursyah, G. M. L., Amalia, T. D. A., Hidayat., Rizkika, O., Marjiyono, M., & Handyarso, A. (2021). Optimasi Kualitas Data Magnetotelurik di Daerah Singkawang dan Sekitarnya Berdasarkan Analisis Koherensi. *Publikasi Khusus Geosains Laboratorium dan Sarana Penyelidikan*, 69–86.

Junursyah, G. M. L., Parlindungan, E., Hidayat, H., & Harja, A. (2022). Reduksi Efek Dimensionalitas 3D pada Data Magnetotelurik Menggunakan Analisis Koherensi, Tren Kurva, dan Skin Depth: Studi Kasus di Pulau Yapen Bagian Selatan dan Sekitarnya, Papua. *Jurnal Geologi dan Sumberdaya Mineral*, 23(4), 247–255. https://doi.org/10.33332/jgsm.geologi.v23i4.712

Junursyah, G. M. L, Fauzhy, M. A., Hidayat, & Harja, A. (2023). Reduksi Efek Dimensionalitas 3D Berdasarkan Analisis Koherensi Pada Data Magnetotelurik Di Daerah Bandung Bagian Timur. *Publikasi Laboratorium dan Sarana Penyelidikan*, 49–60.

Kalev, S. D., & Toor, G. S. (2018). The composition of soils and sediments. *Green Chemistry* (pp. 339–357). Elsevier. https://doi.org/10.1016/B978-0-12-809270-5.00014-5

Keegan-Treloar, R., Irvine, D. J., Solórzano-Rivas, S. C., Werner, A. D., Banks, E. W., & Currell, M. J. (2022). Fault-controlled springs: A review. *Earth-Science Reviews*, 230, 104058. https://doi.org/10.1016/j.earscirev.2022.104058

Kodoatie, R. J. (2021). *Tata Ruang Air Tanah.* Penerbit Andi.

Kurniawan, O., Surya, R. D., & Wargaliyasa, G. (2022). Analisis Fault Fracture Density pada Potensi Panas Bumi NonVulkanik untuk Menentukan Recharge Area; Studi Kasus di Wilayah Lore Lindu, Sulawesi Tengah. *Jurnal Ilmiah*

Geomatika, 2(2), 45–53. https://doi.org/10.31315/imagi.v2i2.9417

Kurniawan, R., Ardi, N. D., & Hidayat, H. (2019). Analisis Penampang Resistivitas 2D Metode Magnetotellurik dan Audio-magnetotellurik Untuk Mengetahui Sistem Petroleum Pada Cekungan Singkawang. *Wahana Fisika*, 4(2), 81–88. https://doi.org/10.17509/wafi.v4i2.21869

Li, J., Wang, W., Cheng, D., Li, Y., Wu, P., & Huang, X. (2021). Hydrogeological Structure Modelling Based on An Integrated Approach Using Multi-Source Data. *Journal of Hydrology*, 600, 126435. https://doi.org/10.1016/j.jhydrol.2021.126435

Montahaei, M. (2022). Audio-Magnetotelluric Modeling for 2D Characterization of Shallow Sedimentary Basins and Groundwater System in Central Zagros, Iran. *Pure and Applied Geophysics*, 179(12), 4567–4594. https://doi.org/10.1007/s00024-022-03181-y

Oktariadi, O., Kasbani, K., & Memed, M. W. (2021). *Geologi Lingkungan Cekungan Bandung*. Badan Geologi.

Pranata, E., Irawati, S. M., & Niasari, S. W. (2017). Magnetotelluric Data Analysis using Swift Skew, Bahr Skew, Polar Diagram, and Phase Tensor: A Case Study in Yellowstone, US. *Proceedings of the Pakistan Academy of Sciences*, 54(3), 311–317. https://www.paspk.org/wp-content/uploads/2017/09/Magnetotelluric-Data-Analysis.pdf

Suhari, S., & Siebenhüner, M. (1993). Environmental geology for land use and regional planning in the Bandung Basin, West Java, Indonesia. *Journal of Southeast Asian Earth Sciences*, 8(1–4), 557–566. https://doi.org/10.1016/0743-9547(93)90053-R

Tripathi, A., Shalivahan, S. S., Bage, A. K., Singh, S., & Yadav, P. K. (2019). Audio-Magnetotelluric Investigation of Bakreswar Geothermal Province, Eastern India. *Journal of Earth System Science*, 128, 102. https://doi.org/10.1007/s12040-019-1115-8

Wu, Q., Li, Y.-B, Mi, H.-Z, Wang, G., & Zhang, Z.-Y. (2023). Simulation and Observations of Audio Magnetotelluric Measurements over Water-Covered Areas. *Minerals*, 13(8), 990. https://doi.org/10.3390/min13080990

Xiao, Q., Cai, X., Liang, G., Xu, X., & Zhang, B. (2011). Application of 2D Magnetotelluric Methods in a Geological Complex Area, Xinjiang, China. *Journal of Applied Geophysics*, 75, 19–30. https://doi.org/10.1016/j.jappgeo.2011.06.007

Xu, Z., Li, G., Xin, H., Tang, J., & Lv, F. (2020). Hydrogeological Prospecting in the Da Qaidam Area of the Qaidam Basin Using the Audio-Frequency Magnetotelluric Method. *Journal of Applied Geophysics*, 182, 104179. https://doi.org/10.1016/j.jappgeo.2020.104179

Xu, Z., Xin, H., Weng, Y., & Li, G. (2023). Hydrogeological Study in Tongchuan City Using the Audio-Frequency Magnetotelluric Method. *Magnetochemistry*, 9(1), 32. https://doi.org/10.3390/magnetochemistry9010032

Zaher, M. A., Younis, A., Shaaban, H., & Mohamaden, M. I. I. (2021). Integration of Geophysical Methods for Groundwater Exploration: A Case Study of El Sheikh Marzouq Area, Farafra Oasis, Egypt. *The Egyptian Journal of Aquatic Research*, 47(2), 239–244. https://doi.org/10.1016/j.ejar.2021.03.001